

Adaptive double-phase ROF model: report on 2D experiments

Wojciech Górný* Michał Lasica† Alexandros Matsoukas‡

September 30, 2025

Abstract

This note reports the results of several numerical experiments involving the adaptive double-phase ROF model in the two-dimensional case. The note is split into two parts; this is the first part.

1 Introduction

Below, we briefly describe some numerical experiments concerning the adaptive double-phase ROF model of image denoising; for the detailed description of the model and the definition of weights or parameters we refer to the introduction of the report file for 1D experiments. The numerical experiments reported here were done using an implementation of the adaptive double-phase ROF model through the accelerated Chambolle–Pock algorithm [1]. The algorithm was implemented in python using the Google Colab platform.

We present the results of image denoising using the double-phase ROF model for several choices of test images, both natural and synthetic, and compare the performance of the model with the classical ROF model and the Huber-ROF model. We present the results visually, as well as compare the values of the measures SSIM [3], PSNR (see e.g. [2]) and the total variation error. The test functions are primarily very simple synthetic data, such as the "double-gradient" image, which highlights specific behavior, as well as standard classical test images such as the "peppers" image, the "Cary Grant" image, the "girlface" and the "schnitzel" image. All these images are currently in public domain.

To illustrate the evaluation of performance of the three models, we provide tables for representative visual experiments where the parameters corresponding to the three ROF models are chosen to optimize the SSIM values. The tables report the number of iterations and the CPU times in seconds that the algorithms needed to drop the normalized error of the primal energy below the error tolerance ϵ . We also refer to the L^2 distance of the denoised version from the noisy image which is approximately the same for each model. In particular, this last benchmark shows that we have a roughly fair comparison between the three models.

*Faculty of Mathematics, Universität Wien, Oskar-Morgerstern-Platz 1, 1090 Vienna, Austria; Faculty of Mathematics, Informatics and Mechanics, University of Warsaw, Banacha 2, 02-097 Warsaw, Poland; wojciech.gorny@univie.ac.at

†Institute of Mathematics of the Polish Academy of Sciences, Śniadeckich 8, 00-656 Warsaw, Poland; mlasica@impan.pl

‡Department of Mathematics, School of Applied Mathematical and Physical Sciences, National Technical University of Athens, Zografou Campus, 157 80 Athens, Greece; alexmatsoukas@mail.ntua.gr

For completeness, we briefly provide some basic notations, as introduced in the report file for 1D experiments. Given the noisy datum g , let u_{ROF} denote the minimizer of the classical ROF model. We define its mollified version by

$$\tilde{u}_{\text{ROF}} = \rho_r * u_{\text{ROF}},$$

where r is the mollification radius. Similarly, we denote the mollified version of the noisy image by

$$\tilde{g} = \rho_r * g.$$

We use the weight w_1 , defined by

$$w_1(x) = W_1(|\nabla \tilde{u}_{\text{ROF}}|(x)), \quad (1)$$

where the function W_1 is given by

$$W_1(x) = \max \left(0, a - b \max \left(x, \frac{a}{2b} \right) \right).$$

When the construction of the weight is based on the mollified function \tilde{u}_{ROF} , we apply directly the above definition. Alternatively, the weight can be constructed in the same manner using either the original minimizer u_{ROF} (without mollification) or the mollified datum \tilde{g} . We present results for these different cases in the experiments with the synthetic "double-gradient" image. For the experiments on natural images, the weight is defined as in (1) with mollification radius $r = 2$ and pair of parameters (a, b) specified in the description of each corresponding experiment.

2 Double Gradient 256×256

Experiment 2.0.1.

1. Weight $w(x) = W_1(|\nabla u_{ROF}|)$;
2. $a = 200, b = 1000$;
3. $\alpha_h = 0.01$;
4. $\sigma = 0.01$;
5. Tolerance level: 10^{-4} ;

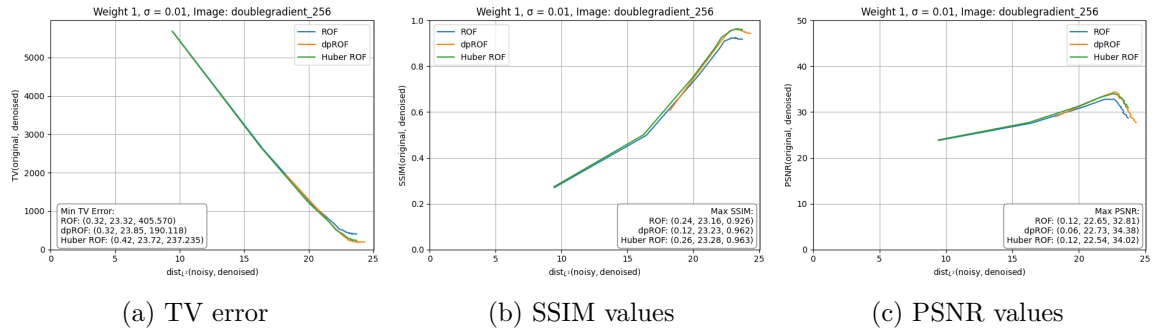


Figure 1: Plots of the metrics with respect to L^2 -distance from the noisy image, for classical ROF, double-phase ROF and Huber ROF ($a_h = 0.01$) with noise level $\sigma = 0.01$.

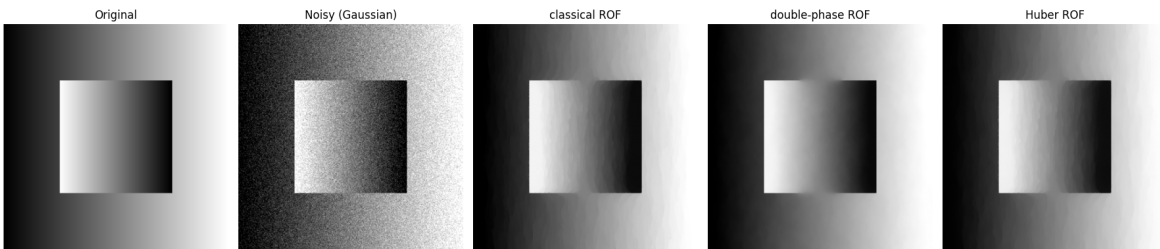


Figure 2: Original and noisy images of double gradient synthetic image, along with the de-noised results corresponding to the maximum SSIM values. The methods shown are: classical ROF ($\lambda = 0.24$), double-phase ROF ($\lambda = 0.12$), and Huber ROF ($\alpha_h = 0.01, \lambda = 0.26$) with $\sigma = 0.01$.

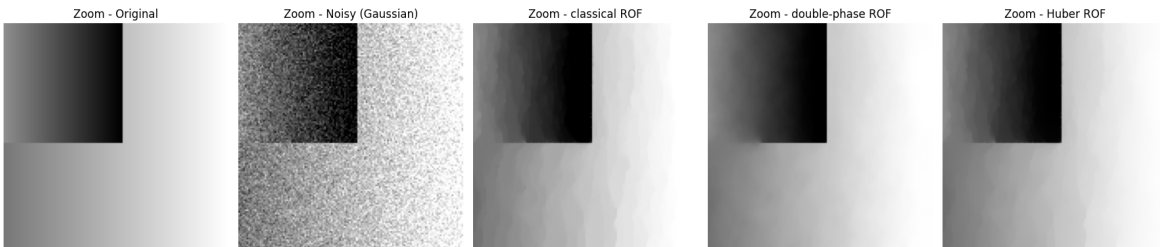


Table 1: Evaluation of performance

error $\epsilon = 10^{-4}$	Classical ROF	Double-phase ROF	Huber ROF
λ	0.24	0.12	0.26
dist_{L^2}	23.16	23.23	23.28
maxSSIM	0.926	0.962	0.963
iterations	1334	583 (+613)	1932
time	18.29s	9.95s (+10.00s)	13.69s

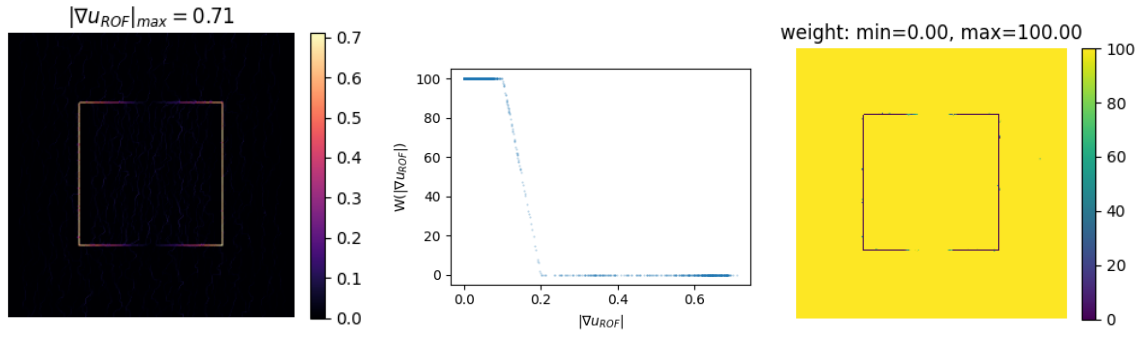


Figure 3: Construction of the weight from gradient of u_{ROF} with $\lambda = 0.12$.

Experiment 2.0.2.

1. Weight $w(x) = W_1(|\nabla \rho_r * g|)$ with $r = 1$;
2. $a = 150, b = 1500$;
3. $\alpha_h = 0.01$;
4. $\sigma = 0.01$;
5. Tolerance level: 10^{-4} ;

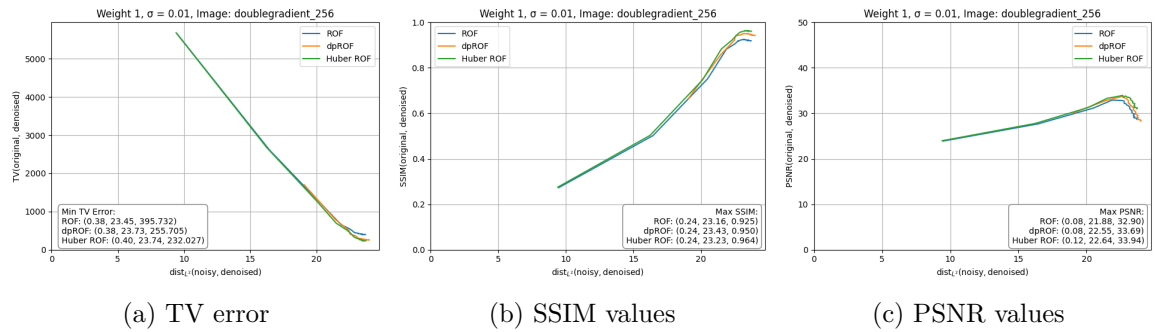


Figure 4: Plots of the metrics with respect to L^2 -distance from the noisy image, for classical ROF, double-phase ROF and Huber ROF ($a_h = 0.01$) with noise level $\sigma = 0.01$.

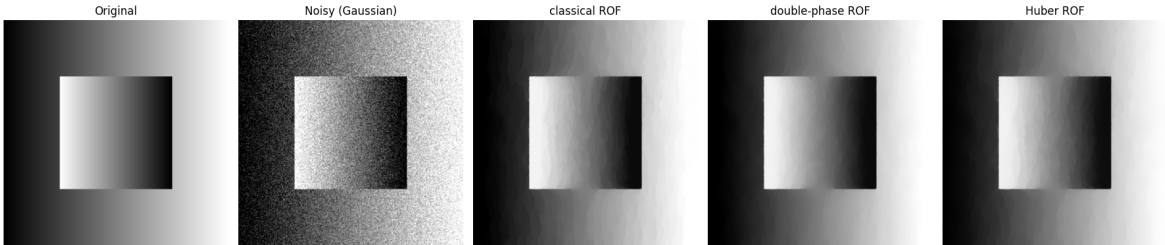


Figure 5: Original and noisy images of double gradient synthetic image, along with the denoised results corresponding to the maximum SSIM values. The methods shown are: classical ROF ($\lambda = 0.24$), double-phase ROF ($\lambda = 0.24$), and Huber ROF ($\alpha_h = 0.01, \lambda = 0.24$) with $\sigma = 0.01$.

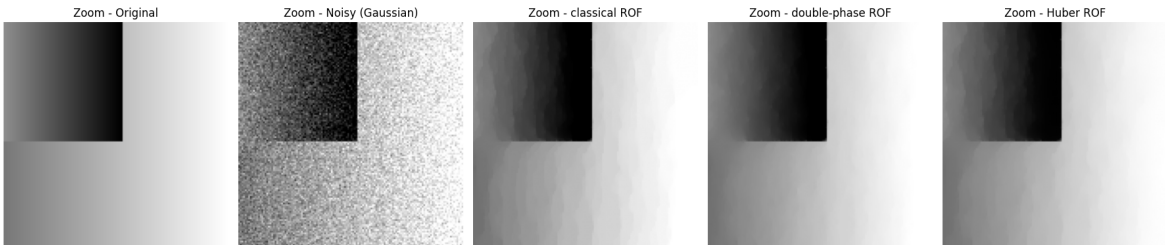


Table 2: Evaluation of performance

error $\epsilon = 10^{-4}$	Classical ROF	Double-phase ROF	Huber ROF
λ	0.24	0.24	0.24
dist_{L^2}	23.16	23.43	23.23
maxSSIM	0.925	0.950	0.964
iterations	1195	963 (+997)	1892
time	14.17s	18.21s (+11.89s)	14.15s

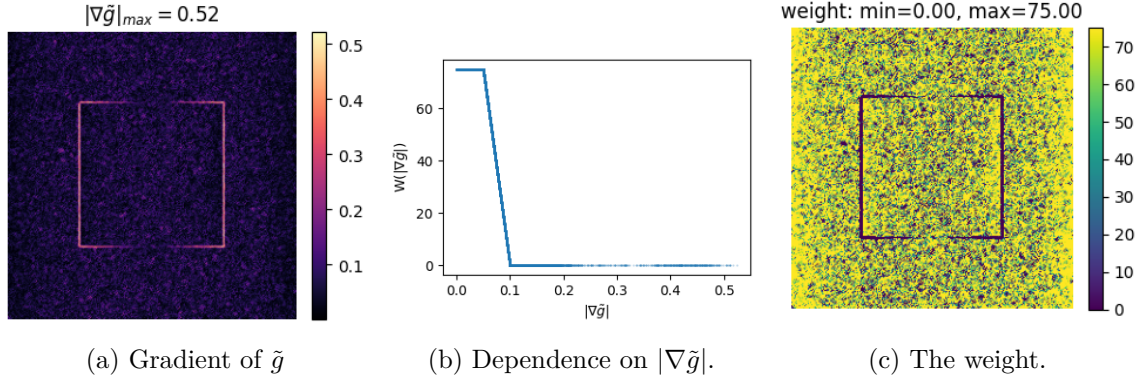


Figure 6: Construction of the weight from gradient of the mollified noisy datum \tilde{g} with $\lambda = 0.24$.

Experiment 2.0.3.

1. Weight $w(x) = W_1(|\nabla \rho_r * u_{ROF}|)$ with $r = 1$;
2. $a = 150, b = 1500$;
3. $\alpha_h = 0.01$;
4. $\sigma = 0.01$;
5. Tolerance level: 10^{-4} ;

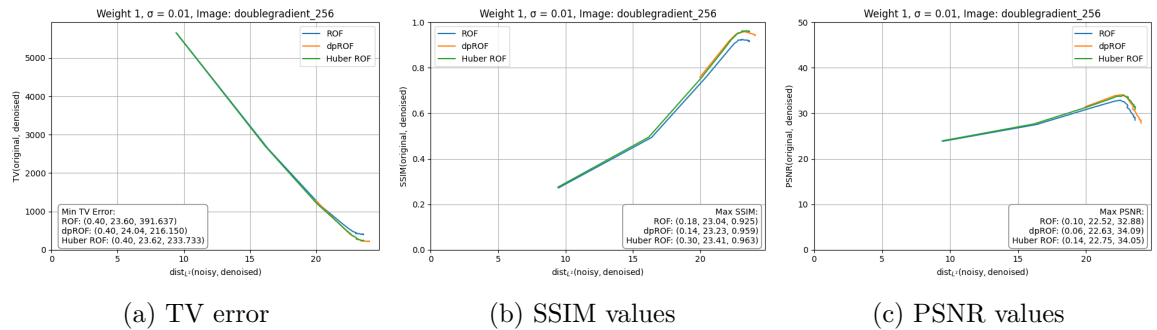


Figure 7: Plots of the metrics with respect to L^2 -distance from the noisy image, for classical ROF, double-phase ROF and Huber ROF ($a_h = 0.01$) with noise level $\sigma = 0.01$.

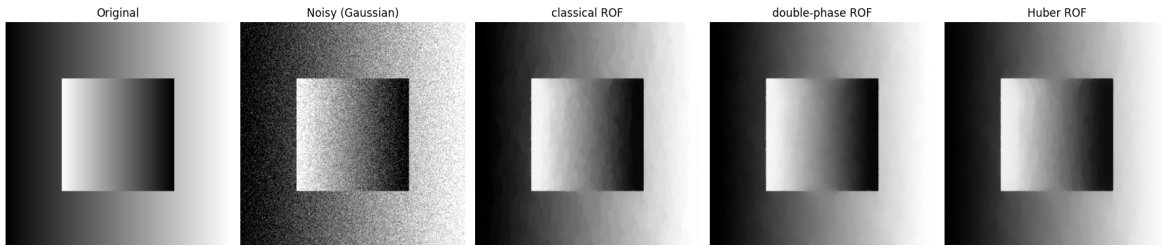


Figure 8: Original and noisy images of double gradient synthetic image, along with the denoised results corresponding to the maximum SSIM values. The methods shown are: classical ROF ($\lambda = 0.18$), double-phase ROF ($\lambda = 0.14$), and Huber ROF ($\alpha_h = 0.01, \lambda = 0.30$) with $\sigma = 0.01$.

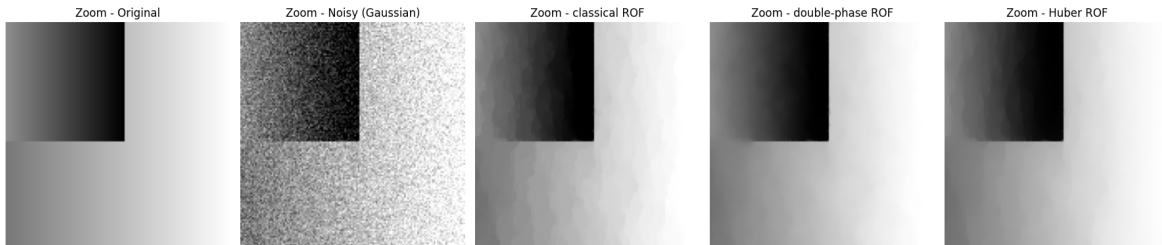


Table 3: Evaluation of performance

error $\epsilon = 10^{-4}$	Classical ROF	Double-phase ROF	Huber ROF
λ	0.18	0.14	0.30
dist_{L^2}	23.04	23.23	23.41
maxSSIM	0.925	0.959	0.963
iterations	951	527 (+838)	2078
time	13.48s	10.68s (+15.44s)	15.94s

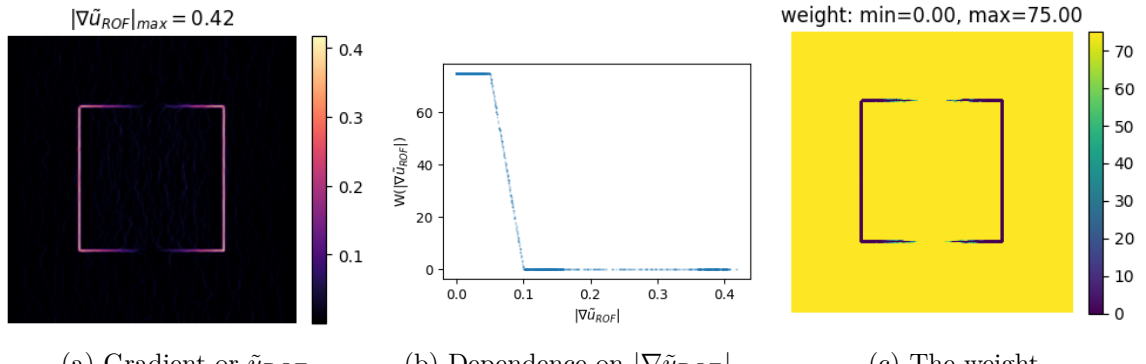


Figure 9: Construction of the weight from gradient of \tilde{u}_{ROF} with $\lambda = 0.14$.

Experiment 2.0.4.

1. Weight $w(x) = W_1(|\nabla \rho_r * u_{ROF}|)$ with $r = 2$;
2. $a = 90, b = 1500$;
3. $\alpha_h = 0.01$;
4. $\sigma = 0.01$;
5. Tolerance level: 10^{-4} ;

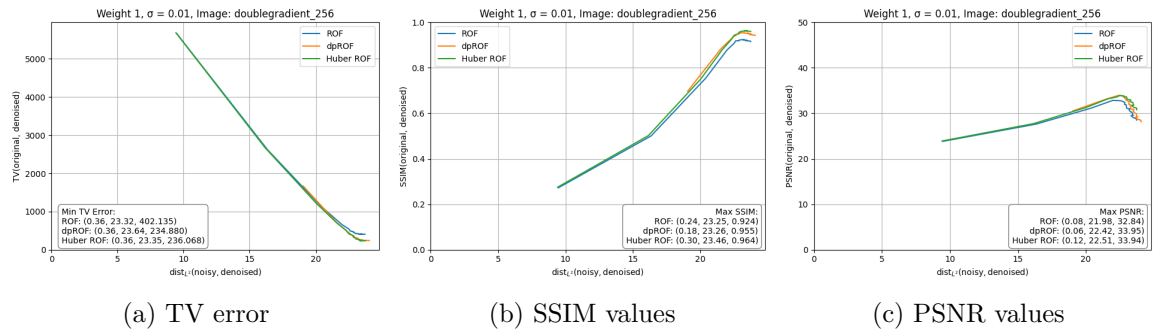


Figure 10: Plots of the metrics with respect to L^2 -distance from the noisy image, for classical ROF, double-phase ROF and Huber ROF ($a_h = 0.01$) with noise level $\sigma = 0.01$.

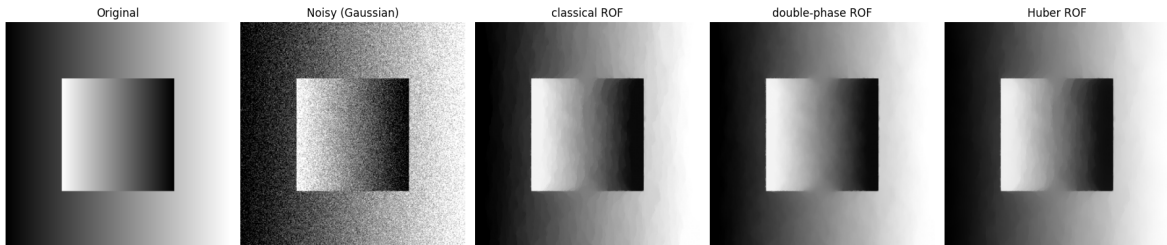


Figure 11: Original and noisy images of double gradient synthetic image, along with the denoised results corresponding to the maximum SSIM values. The methods shown are: classical ROF ($\lambda = 0.24$), double-phase ROF ($\lambda = 0.18$), and Huber ROF ($\alpha_h = 0.01, \lambda = 0.30$) with $\sigma = 0.01$.

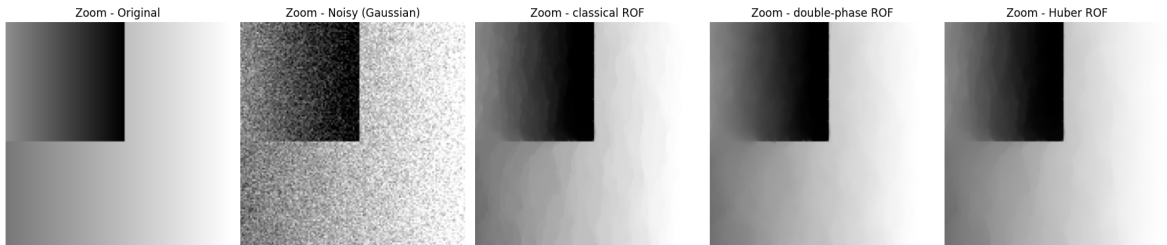
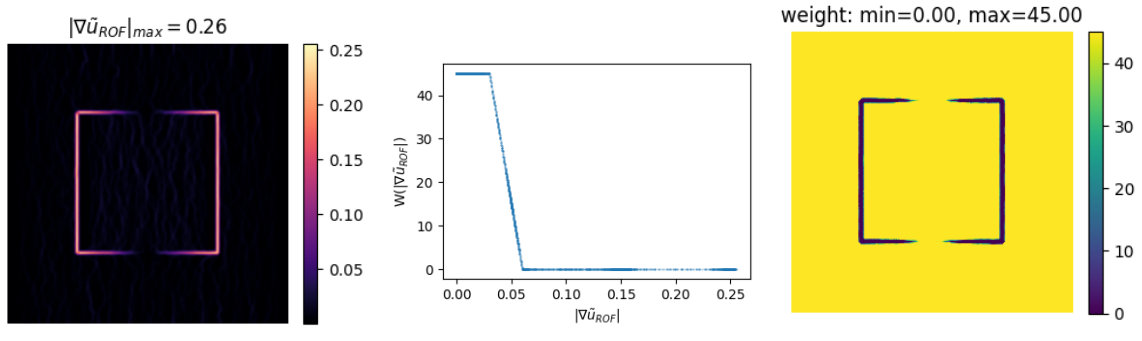


Table 4: Evaluation of performance

error $\epsilon = 10^{-4}$	Classical ROF	Double-phase ROF	Huber ROF
λ	0.24	0.18	0.30
dist_{L^2}	23.25	23.26	23.46
maxSSIM	0.924	0.955	0.964
iterations	1215	906 (+992)	2081
time	13.42s	16.60s (+11.50s)	14.80s



(a) Gradient or \tilde{u}_{ROF}

(b) Dependence on $|\nabla \tilde{u}_{\text{ROF}}|$.

(c) The weight.

Figure 12: Construction of the weight from gradient of \tilde{u}_{ROF} with $\lambda = 0.18$.

3 Peppers 256×256

Experiment 3.0.1.

1. $a = 50, b = 1000$;
2. $\alpha_h = 0.01$;
3. $\sigma = 0.01, 0.04$;
4. Tolerance level: 10^{-4} ;

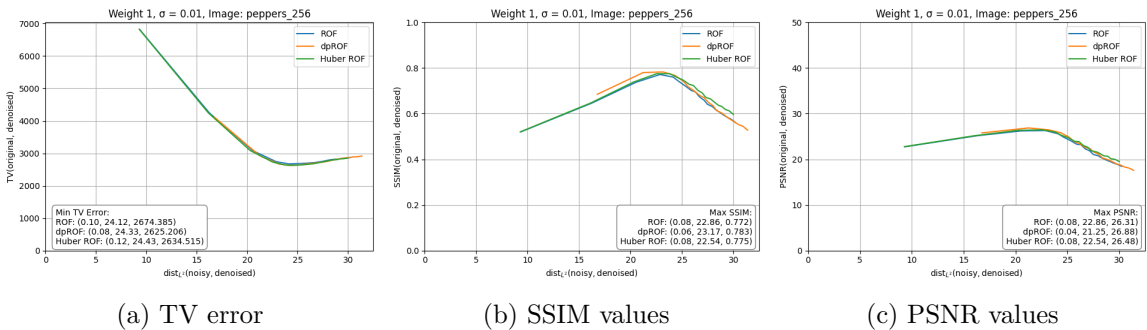


Figure 13: Plots of the metrics with respect to L^2 -distance from the noisy image, for classical ROF, double-phase ROF and Huber ROF ($a_h = 0.01$) with noise level $\sigma = 0.01$.

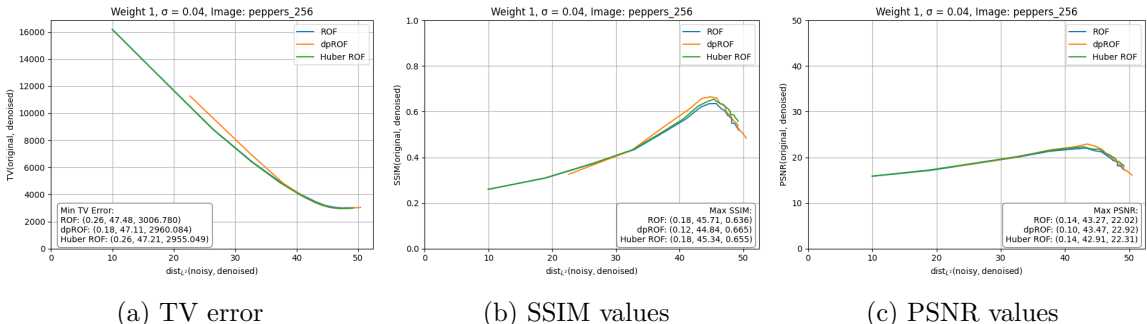


Figure 14: Plots of the metrics with respect to L^2 -distance from the noisy image, for classical ROF, double-phase ROF and Huber ROF ($a_h = 0.01$) with noise level $\sigma = 0.04$.

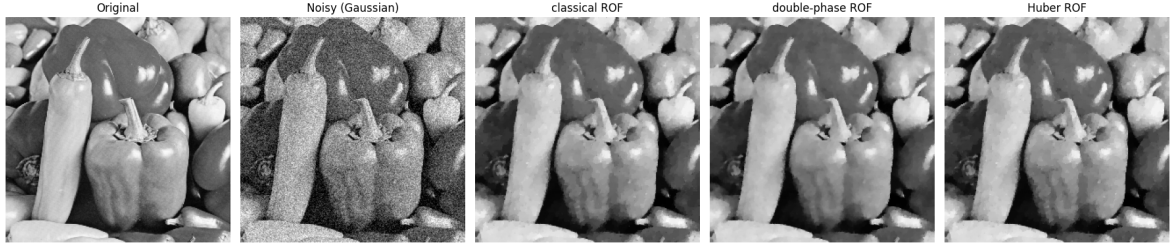


Figure 15: Original and noisy images of peppers, along with the denoised results corresponding to the maximum SSIM values. The methods shown are: classical ROF ($\lambda = 0.08$), double-phase ROF ($\lambda = 0.06$), and Huber ROF ($\alpha_h = 0.01, \lambda = 0.08$) with $\sigma = 0.01$.

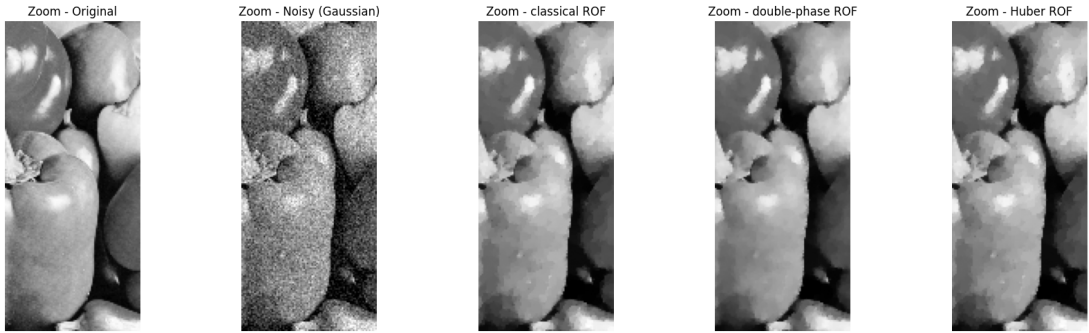
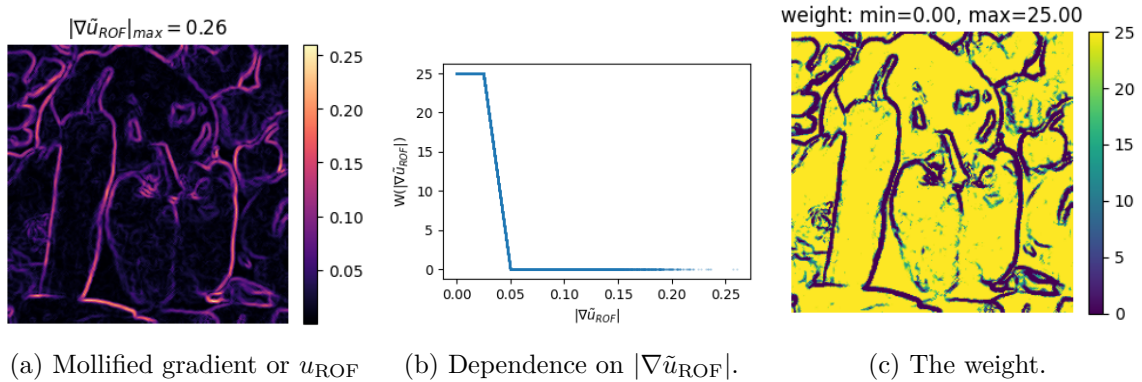


Table 5: Evaluation of performance

error $\epsilon = 10^{-4}$	Classical ROF	Double-phase ROF	Huber ROF
λ	0.08	0.06	0.08
$dist_{L^2}$	22.86	23.17	22.54
maxSSIM	0.772	0.783	0.775
iterations	364	267 (+295)	998
time	8.01s	4.52s (+12.89s)	5.52s



(a) Mollified gradient or u_{ROF} (b) Dependence on $|\nabla \tilde{u}_{\text{ROF}}|$. (c) The weight.

Figure 16: Construction of the weight from mollified gradient of u_{ROF} with $\lambda = 0.06$.

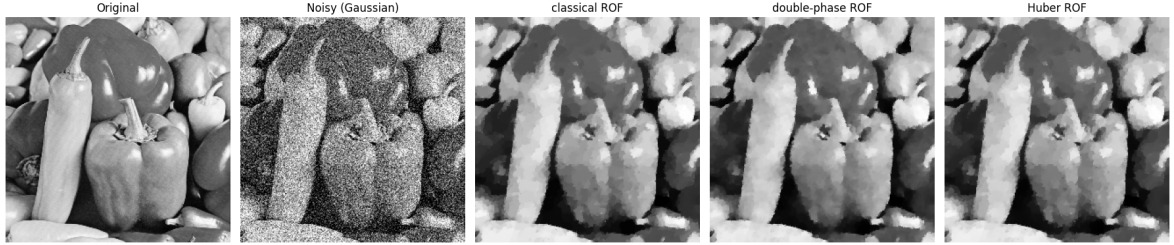


Figure 17: Original and noisy images of peppers, along with the denoised results corresponding to the maximum SSIM values. The methods shown are: classical ROF ($\lambda = 0.18$), double-phase ROF ($\lambda = 0.12$), and Huber ROF ($\alpha_h = 0.01, \lambda = 0.18$) with $\sigma = 0.04$.

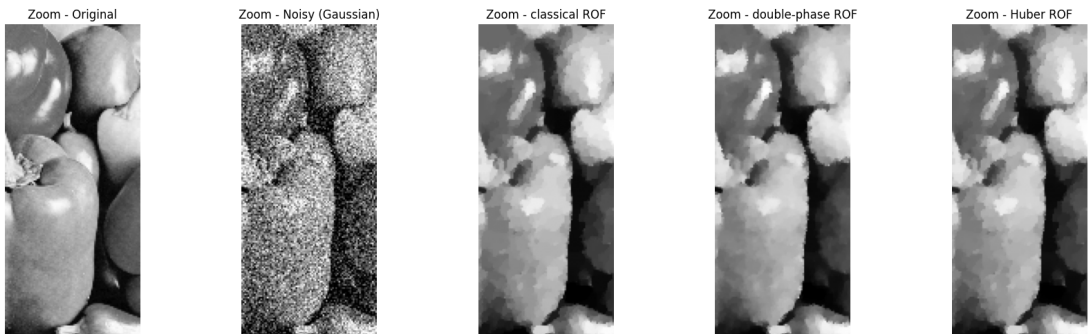


Table 6: Evaluation of performance

error $\epsilon = 10^{-4}$	Classical ROF	Double-phase ROF	Huber ROF
λ	0.18	0.12	0.18
dist_{L^2}	45.71	44.84	45.34
maxSSIM	0.636	0.665	0.655
iterations	606	356 (+401)	1346
time	9.75s	5.81s (+8.53s)	8.45s

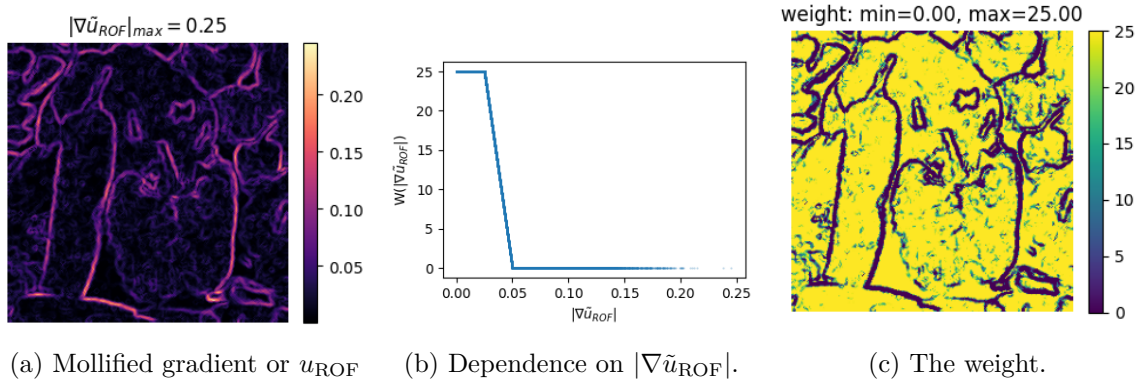


Figure 18: Construction of the weight from mollified gradient of u_{ROF} with $\lambda = 0.12$.

Experiment 3.0.2.

1. $a = 60, b = 1200;$
2. $\alpha_h = 0.01;$
3. $\sigma = 0.01;$
4. Tolerance level: $10^{-4};$

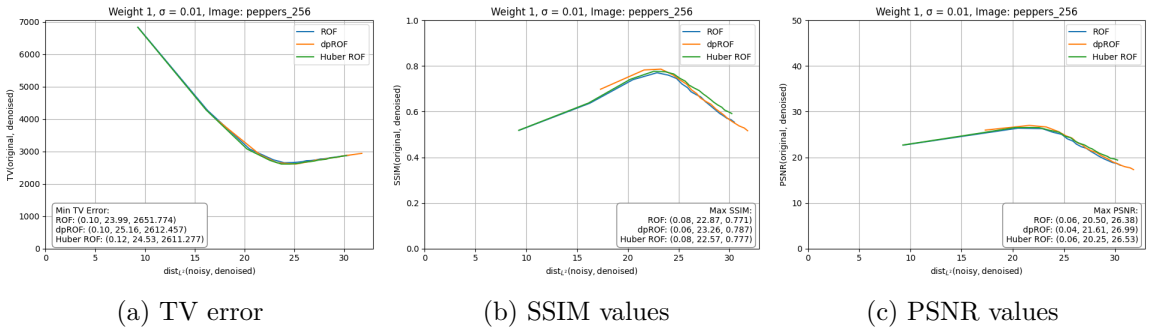


Figure 19: Plots of the metrics with respect to L^2 -distance from the noisy image, for classical ROF, double-phase ROF and Huber ROF ($a_h = 0.01$) with noise level $\sigma = 0.01$.

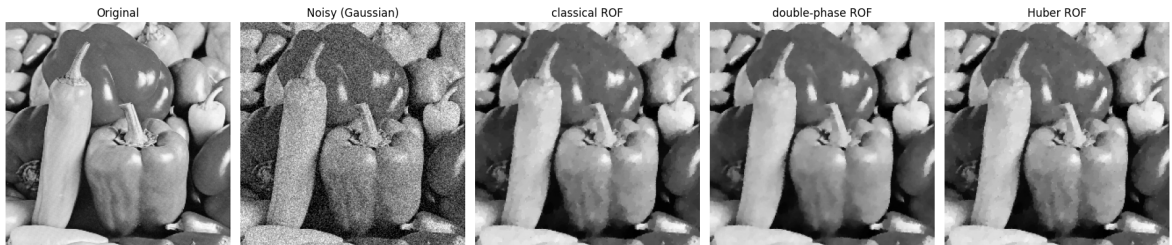


Figure 20: Original and noisy images of peppers, along with the denoised results corresponding to the maximum SSIM values. The methods shown are: classical ROF ($\lambda = 0.08$), double-phase ROF ($\lambda = 0.06$), and Huber ROF ($\alpha_h = 0.01, \lambda = 0.08$) with $\sigma = 0.01$.



Table 7: Evaluation of performance

error $\epsilon = 10^{-4}$	Classical ROF	Double-phase ROF	Huber ROF
λ	0.08	0.06	0.08
dist_{L^2}	22.87	23.26	22.57
maxSSIM	0.771	0.787	0.777
iterations	385	243 (+304)	1021
time	13.72s	5.28s (+8.22s)	6.43s

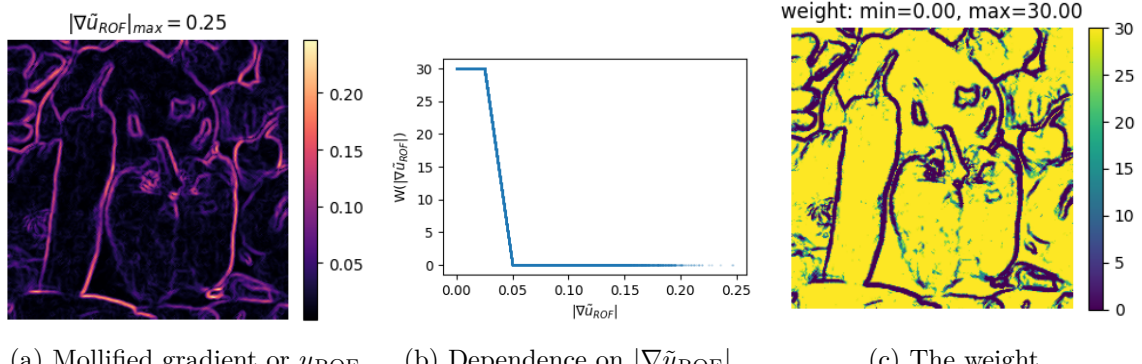


Figure 21: Construction of the weight from mollified gradient of u_{ROF} with $\lambda = 0.06$.

Experiment 3.0.3.

1. $a = 60, b = 1500;$
2. $\alpha_h = 0.01;$
3. $\sigma = 0.04;$
4. Tolerance level: $10^{-4};$

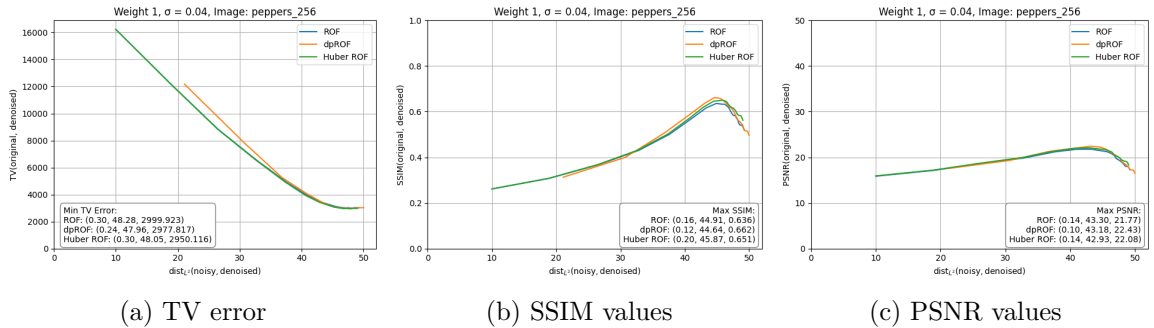


Figure 22: Plots of the metrics with respect to L^2 -distance from the noisy image, for classical ROF, double-phase ROF and Huber ROF ($a_h = 0.01$) with noise level $\sigma = 0.04$.

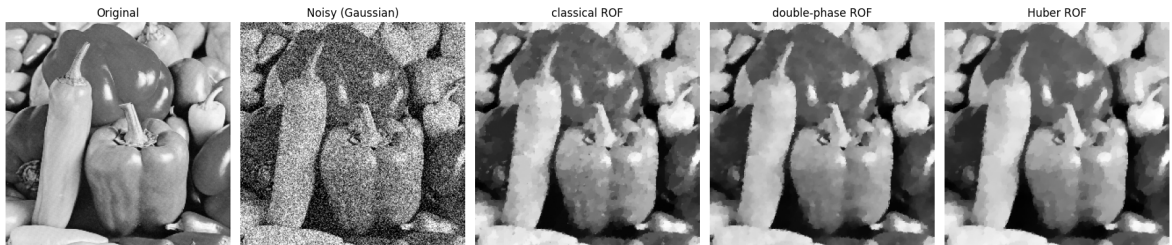


Figure 23: Original and noisy images of peppers, along with the denoised results corresponding to the maximum SSIM values. The methods shown are: classical ROF ($\lambda = 0.16$), double-phase ROF ($\lambda = 0.12$), and Huber ROF ($\alpha_h = 0.01, \lambda = 0.20$) with $\sigma = 0.04$.

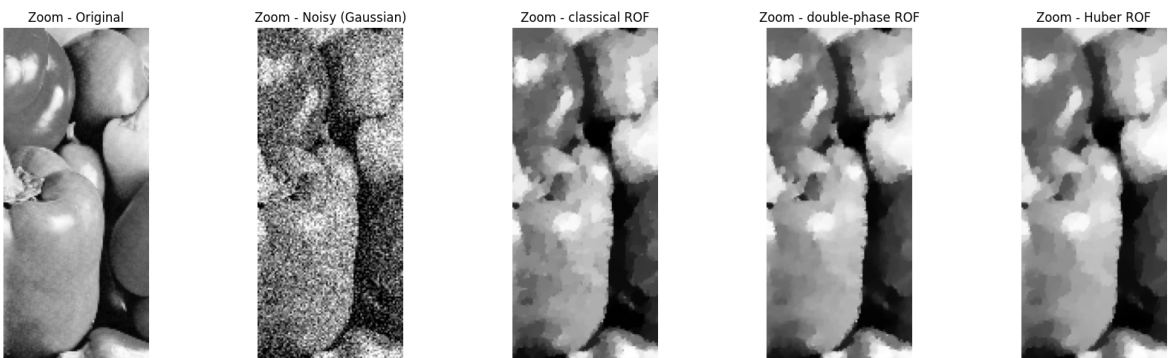
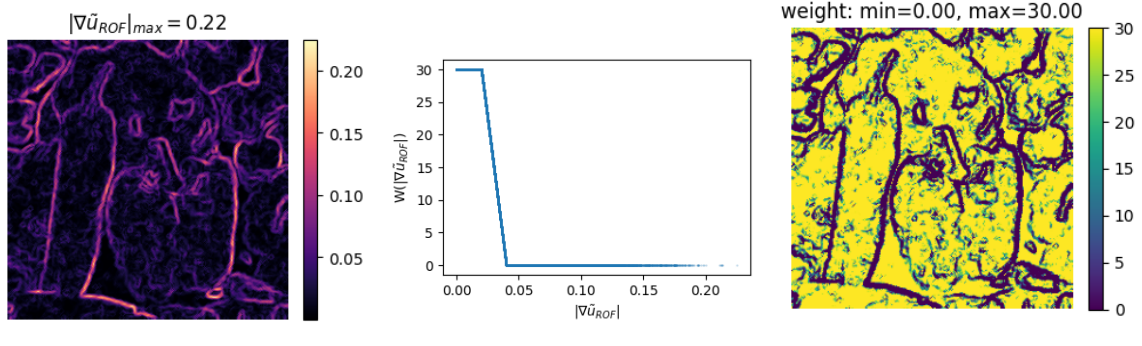


Table 8: Evaluation of performance

error $\epsilon = 10^{-4}$	Classical ROF	Double-phase ROF	Huber ROF
λ	0.16	0.12	0.20
dist_{L^2}	44.91	44.64	45.87
maxSSIM	0.636	0.662	0.651
iterations	544	377 (+405)	1432
time	10.46s	5.88s (+8.75s)	10.53s



(a) Mollified gradient or u_{ROF} (b) Dependence on $|\nabla \tilde{u}_{\text{ROF}}|$. (c) The weight.

Figure 24: Construction of the weight from mollified gradient of u_{ROF} with $\lambda = 0.12$.

4 Cary Grant 512×512

Experiment 4.0.1.

1. $a = 50, b = 1000$;
2. $\alpha_h = 0.005, 0.01$;
3. $\sigma = 0.01, 0.04, 0.07$;
4. Tolerance level: 10^{-4} ;

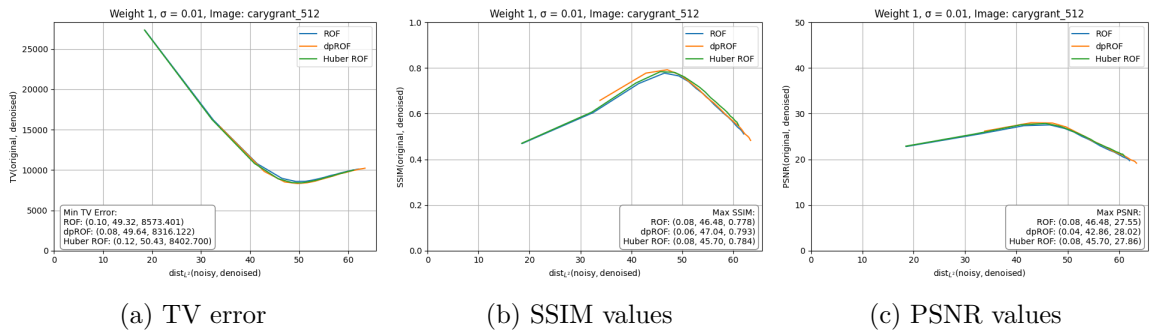


Figure 25: Plots of the metrics with respect to L^2 -distance from the noisy image, for classical ROF, double-phase ROF and Huber ROF ($a_h = 0.01$) with noise level $\sigma = 0.01$.

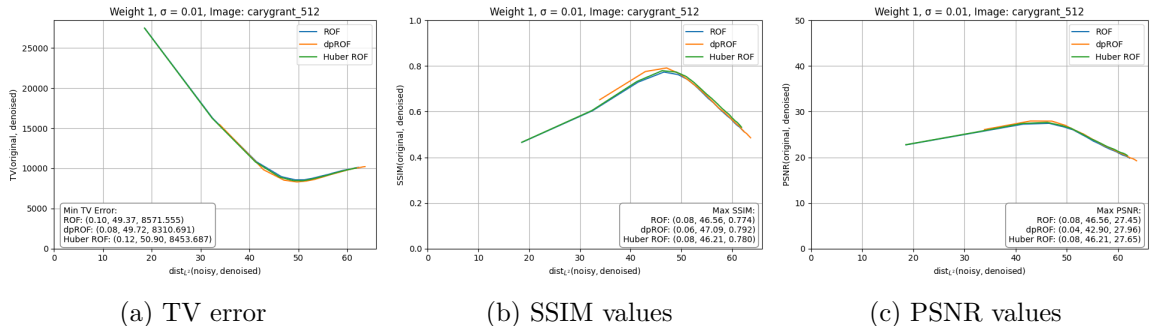


Figure 26: Plots of the metrics with respect to L^2 -distance from the noisy image, for classical ROF, double-phase ROF and Huber ROF ($a_h = 0.005$) with noise level $\sigma = 0.01$.

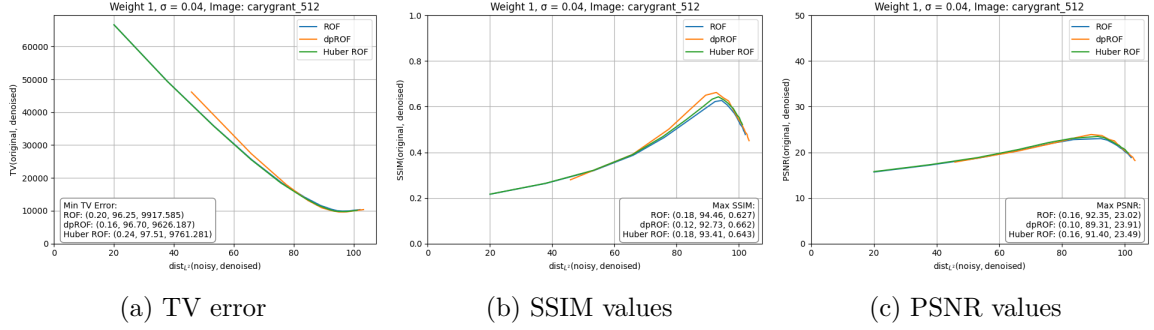


Figure 27: Plots of the metrics with respect to L^2 -distance from the noisy image, for classical ROF, double-phase ROF and Huber ROF ($a_h = 0.01$) with noise level $\sigma = 0.04$.

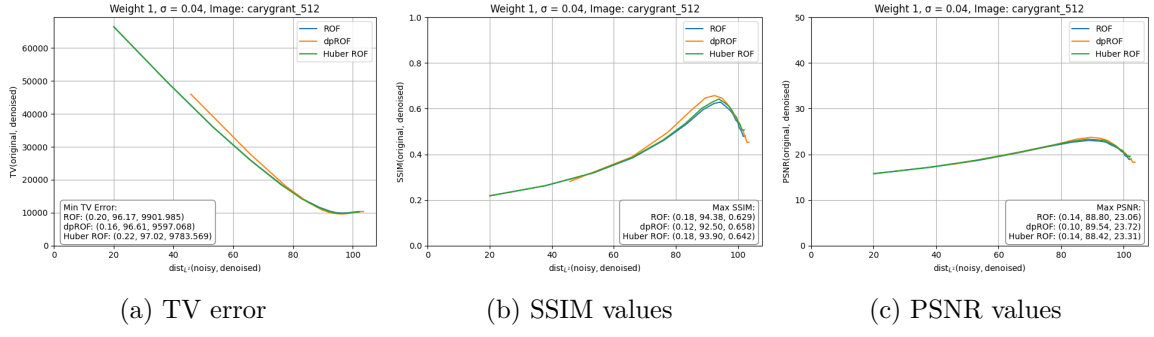


Figure 28: Plots of the metrics with respect to L^2 -distance from the noisy image, for classical ROF, double-phase ROF and Huber ROF ($a_h = 0.005$) with noise level $\sigma = 0.04$.

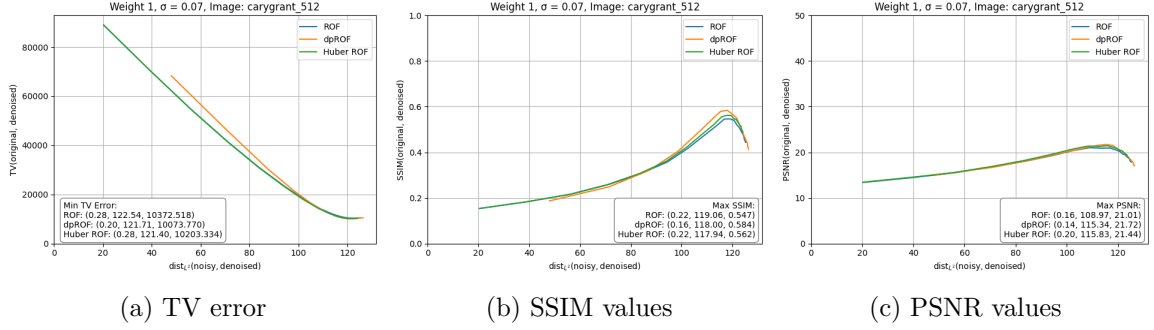


Figure 29: Plots of the metrics with respect to L^2 -distance from the noisy image, for classical ROF, double-phase ROF and Huber ROF ($a_h = 0.01$) with noise level $\sigma = 0.07$.



Figure 30: Original and noisy images of Cary Grant, along with the denoised results corresponding to the maximum SSIM values. The methods shown are: classical ROF ($\lambda = 0.06$), double-phase ROF ($\lambda = 0.08$), and Huber ROF ($\alpha_h = 0.01, \lambda = 0.08$) with $\sigma = 0.01$.

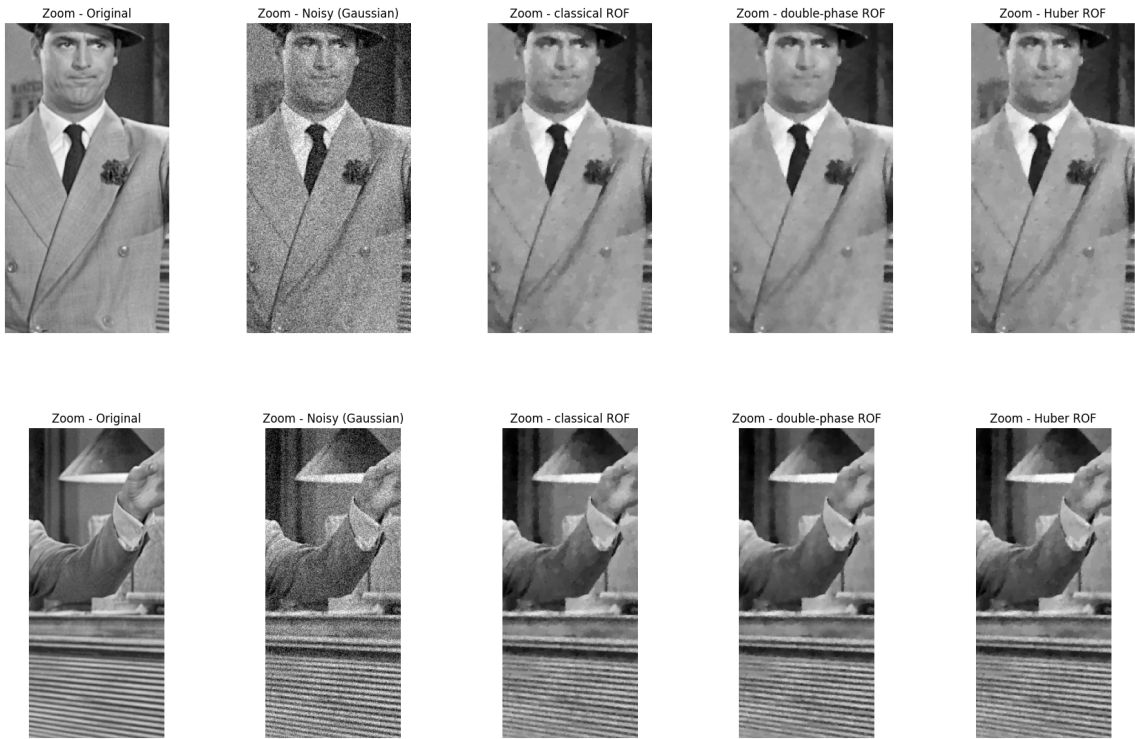
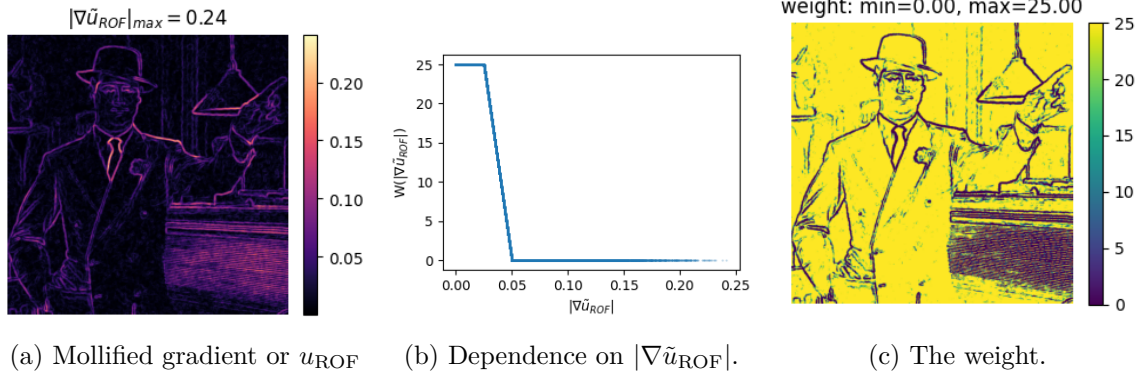


Table 9: Evaluation of performance

error $\epsilon = 10^{-4}$	Classical ROF	Double-phase ROF	Huber ROF
λ	0.08	0.06	0.08
dist L^2	46.48	47.04	45.70
maxSSIM	0.778	0.793	0.784
iterations	490	313 (+347)	1192
time	17.84s	20.90s (+22.90s)	45.70s

(a) Mollified gradient or u_{ROF} (b) Dependence on $|\nabla \tilde{u}_{\text{ROF}}|$.

(c) The weight.

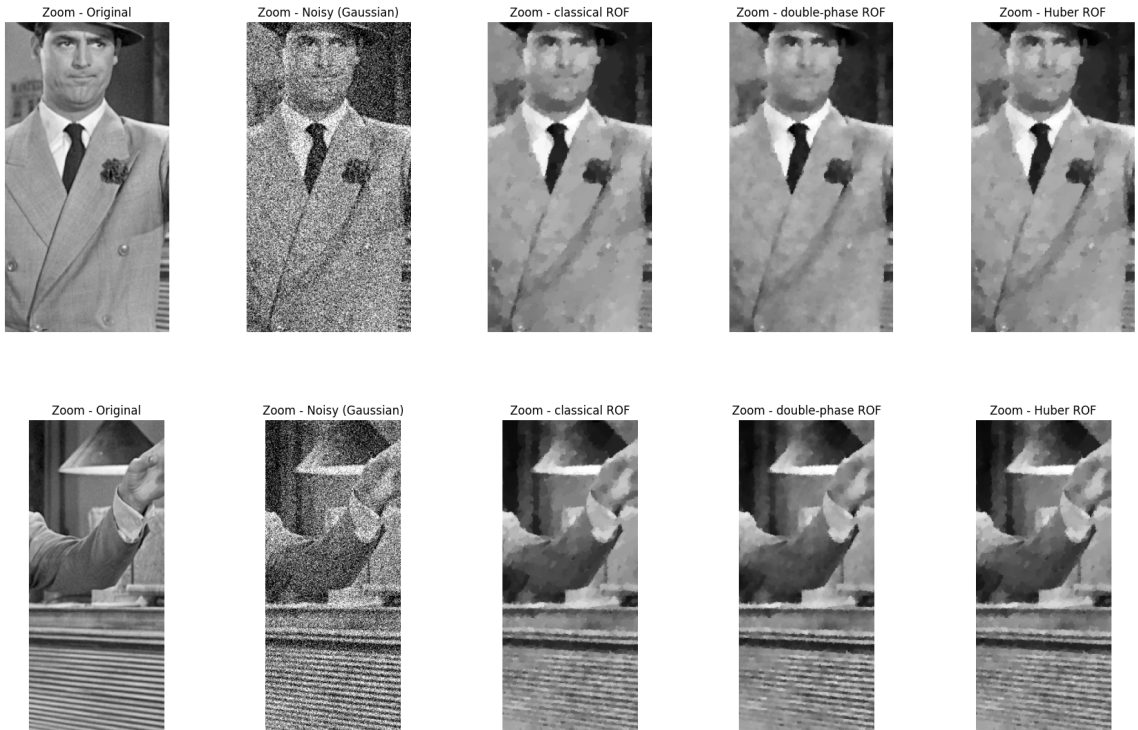
Figure 31: Construction of the weight from mollified gradient of u_{ROF} with $\lambda = 0.06$.Figure 32: Original and noisy images of Cary Grant, along with the denoised results corresponding to the maximum SSIM values. The methods shown are: classical ROF ($\lambda = 0.18$), double-phase ROF ($\lambda = 0.12$), and Huber ROF ($\alpha_h = 0.01, \lambda = 0.18$) with $\sigma = 0.04$.

Table 10: Evaluation of performance

error $\epsilon = 10^{-4}$	Classical ROF	Double-phase ROF	Huber ROF
λ	0.18	0.12	0.18
dist_{L^2}	94.46	92.73	93.41
maxSSIM	0.627	0.662	0.643
iterations	798	449 (+482)	1596
time	23.24s	30.59s (+8.65s)	45.27s

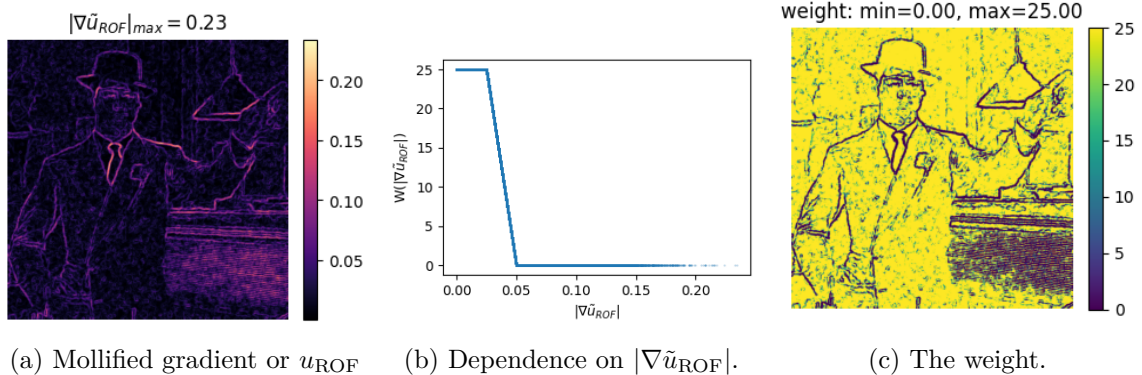


Figure 33: Construction of the weight from mollified gradient of u_{ROF} with $\lambda = 0.12$.

Experiment 4.0.2.

1. $a = 60, b = 1500$;
2. $\alpha_h = 0.01$;
3. $\sigma = 0.01, 0.04, 0.07$;
4. Tolerance level: 10^{-4} ;

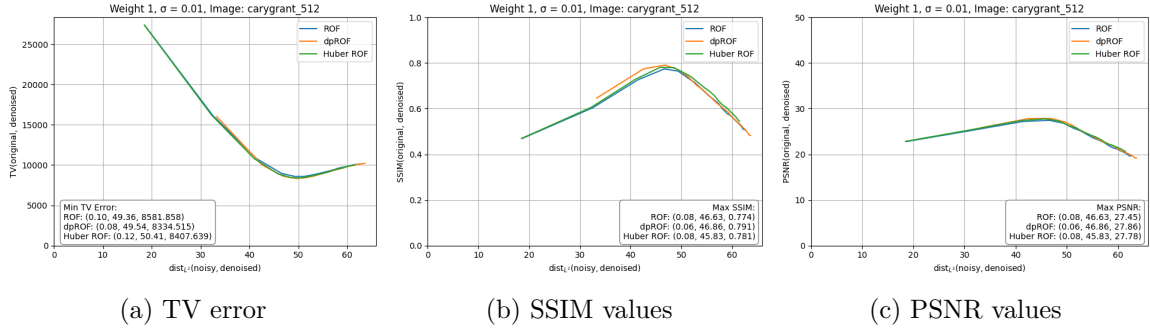


Figure 34: Plots of the metrics with respect to L^2 -distance from the noisy image, for classical ROF, double-phase ROF and Huber ROF ($a_h = 0.01$) with noise level $\sigma = 0.01$.

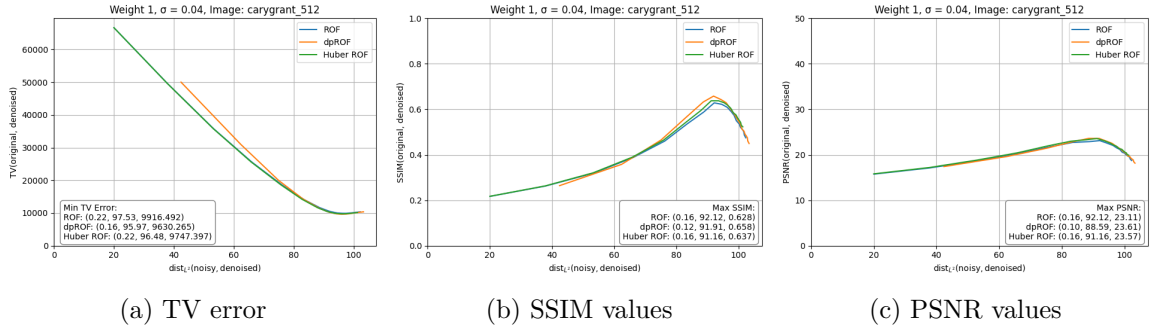


Figure 35: Plots of the metrics with respect to L^2 -distance from the noisy image, for classical ROF, double-phase ROF and Huber ROF ($a_h = 0.01$) with noise level $\sigma = 0.04$.

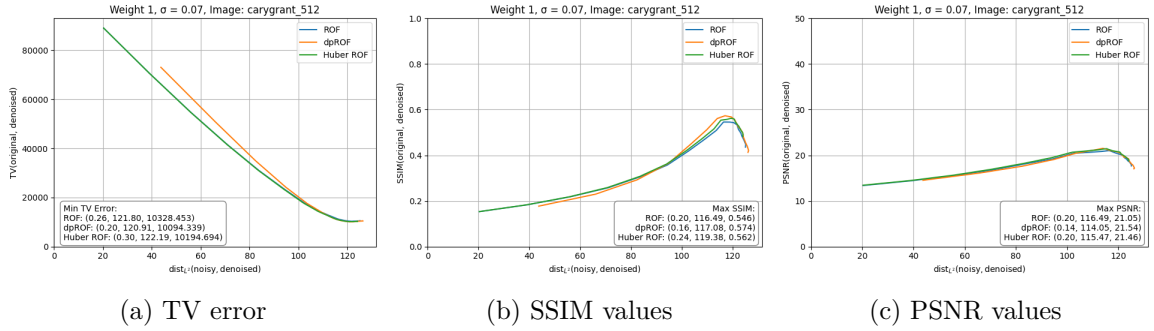


Figure 36: Plots of the metrics with respect to L^2 -distance from the noisy image, for classical ROF, double-phase ROF and Huber ROF ($a_h = 0.01$) with noise level $\sigma = 0.07$.



Figure 37: Original and noisy images of Cary Grant, along with the denoised results corresponding to the maximum SSIM values. The methods shown are: classical ROF ($\lambda = 0.06$), double-phase ROF ($\lambda = 0.08$), and Huber ROF ($\alpha_h = 0.01, \lambda = 0.08$) with $\sigma = 0.01$.

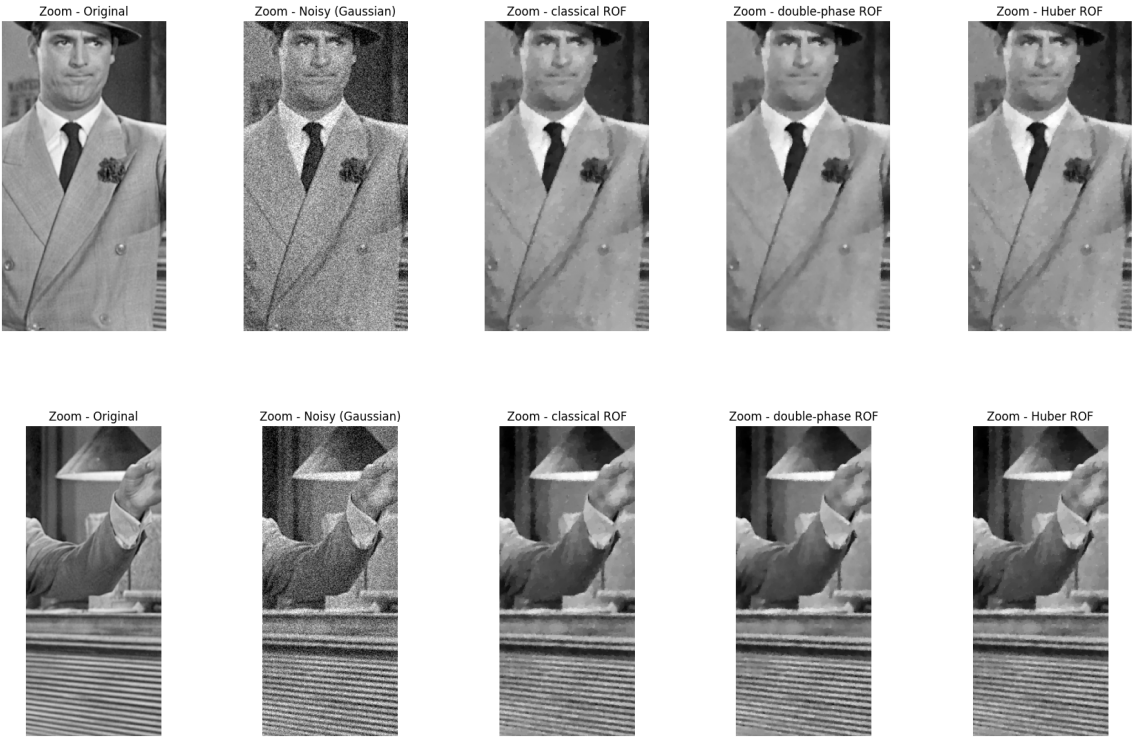
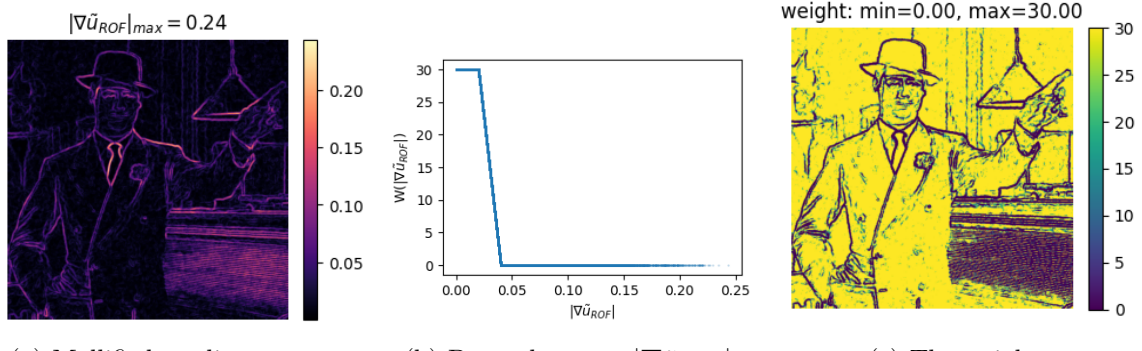


Table 11: Evaluation of performance

error $\epsilon = 10^{-4}$	Classical ROF	Double-phase ROF	Huber ROF
λ	0.08	0.06	0.08
dist_{L^2}	46.63	46.86	45.83
maxSSIM	0.774	0.791	0.781
iterations	484	322 (+347)	1202
time	15.90s	22.27s (+22.90s)	45.83s



(a) Mollified gradient or u_{ROF} (b) Dependence on $|\nabla \tilde{u}_{\text{ROF}}|$. (c) The weight.

Figure 38: Construction of the weight from mollified gradient of u_{ROF} with $\lambda = 0.06$.

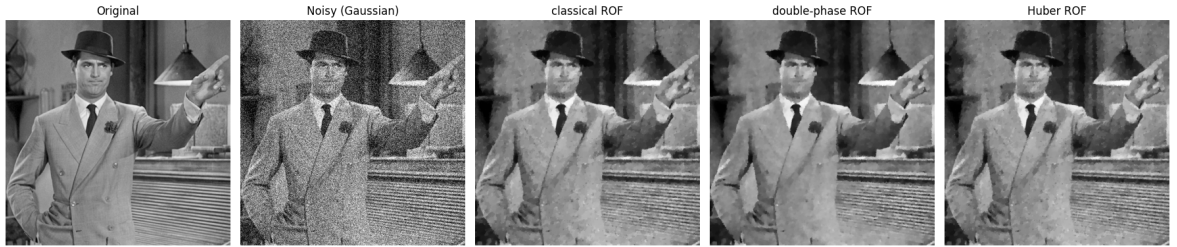


Figure 39: Original and noisy images of Cary Grant, along with the denoised results corresponding to the maximum SSIM values. The methods shown are: classical ROF ($\lambda = 0.16$), double-phase ROF ($\lambda = 0.12$), and Huber ROF ($\alpha_h = 0.01, \lambda = 0.16$) with $\sigma = 0.04$.



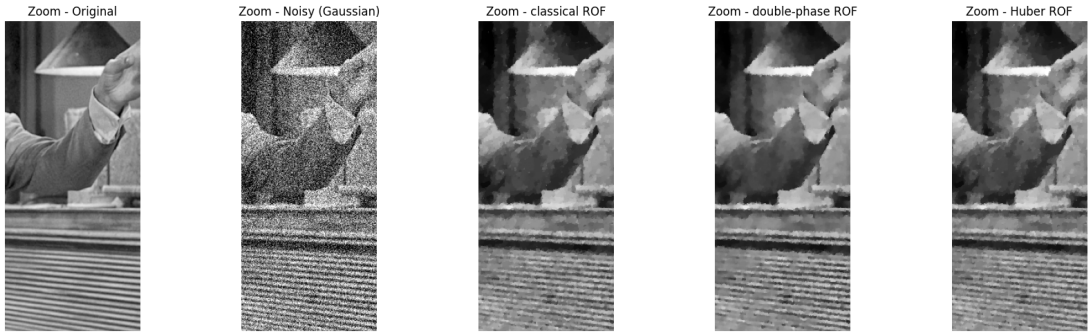
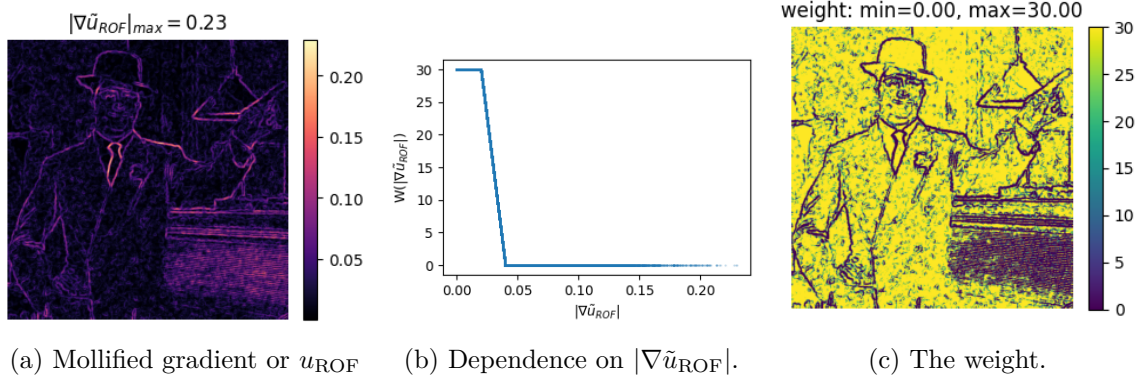


Table 12: Evaluation of performance

error $\epsilon = 10^{-4}$	Classical ROF	Double-phase ROF	Huber ROF
λ	0.16	0.12	0.16
dist_{L^2}	92.12	91.91	91.16
maxSSIM	0.628	0.658	0.637
iterations	706	448 (+500)	1456
time	28.32s	33.73s (+17.62s)	45.53s



(a) Mollified gradient or u_{ROF} (b) Dependence on $|\nabla \tilde{u}_{\text{ROF}}|$. (c) The weight.

Figure 40: Construction of the weight from mollified gradient of u_{ROF} with $\lambda = 0.12$.

Acknowledgments. The work of the first author has been supported by the Austrian Science Fund (FWF), grants 10.55776/ESP88 and 10.55776/I5149. The second author has been partially supported by the grant 2024/55/D/ST1/03055 of the National Science Centre (NCN), Poland. The third author has been partially supported by the Special Account for Research Funding of the National Technical University of Athens.

References

- [1] Antonin Chambolle, Thomas Pock. A first-order primal-dual algorithm for convex problems with applications to imaging. *J. Math. Imaging Vis.* 40 (2011) pp. 120–145. doi: 10.1007/s10851-010-0251-1.
- [2] David Salomon. *Data Compression: The Complete Reference (4 ed.)*. Springer (2007).
- [3] Z. Wang, A.C. Bovik, H.R. Sheikh, E.P. Simoncelli. Image quality assessment: from error visibility to structural similarity. *IEEE Transactions on Image Processing* 13 (2004) pp. 600–612.